Space-frequency-polarization-division multiplexed wireless communication system using anisotropic space-time-coding digital metasurface

Jun Chen Ke
State Key Laboratory of Millimeter Waves, Southeast University
Xiangyu Chen
Southeast University
Wankai Tang
Southeast University https://orcid.org/0000-0002-1751-3457
Ming Zheng Chen
State Key Laboratory of Millimeter Waves, Southeast University
Lei Zhang
Southeast University https://orcid.org/0000-0002-8791-6374
Li Wang
Southeast University
Jun Yan Dai
Southeast University
Jin Yang
Southeast University
Jun Wei Zhang
Southeast University
Lijie Wu
Southeast University
Qiang Cheng
Southeast University https://orcid.org/0000-0002-2442-8357
Shi Jin
Southeast University https://orcid.org/0000-0003-0271-6021
Tie Jun Cui (tjcui@seu.edu.cn)
Southeast University https://orcid.org/0000-0002-5862-1497

Article

Keywords: Polarization-division multiplexing, frequency-division multiplexing, space-division multiplexing, space-time-coding, wireless communication

Posted Date: April 14th, 2022

DOI: https://doi.org/10.21203/rs.3.rs-1509959/v1

Space-frequency-polarization-division multiplexed wireless communication system using anisotropic space-time-coding digital metasurface

Jun Chen Ke[1,2], Xiangyu Chen[3], Wankai Tang[3], Ming Zheng Chen[1,2], Lei Zhang[1,2], Li Wang[1,2], Jun Yan Dai[1,2], Jin Yang[4], Jun Wei Zhang[1,2], Lijie Wu[1,2], Qiang Cheng[1,2,*], Shi Jin[3,*], and Tie Jun Cui[1,2,*]

[1] Institute of Electromagnetic Space, Southeast University, Nanjing 210096, China
[2] State Key Laboratory of Millimeter Waves, Southeast University, Nanjing 210096, China
[3] National Mobile Communications Research Laboratory, Southeast University, Nanjing 210096, China
[4] Southeast University Wuxi Campus, Wuxi 214061, China

* Corresponding authors.
E-mail: qiangcheng@seu.edu.cn; jinshi@seu.edu.cn; tjcui@seu.edu.cn

Abstract

In the past years, wireless communications based on digital coding metasurfaces have gained research interests owing to the simplified architectures and low costs. However, in most of the metasurface-based wireless systems, single-polarization scenario is used, limiting the channel capacities. To solve the problem, multiplexing methods have been adopted, but the system complexity is inevitably increased. Here, a space-frequency-polarization-division multiplexed wireless communication system is proposed using an anisotropic space-time-coding (STC) digital metasurface. By separately designing time-varying control voltage sequences for differently oriented varactor diodes integrated on the metasurface, we achieve frequency-polarization-division multiplexed modulations. By further introducing different time-delay gradients to the control voltage sequences in two polarization directions, we successfully obtain space-frequency-polarization-division multiplexed modulations to realize new-architecture wireless communication system. The new communication system is designed with compact dual-polarized meta-elements, and can improve the channel capacity and space

utilization. Experimental results demonstrate high-performance and real-time transmission capability of the proposed communication system, confirming the potential applications in multiple-user collaborative wireless communications.

Keywords

Polarization-division multiplexing, frequency-division multiplexing, space-division multiplexing, space-time-coding, wireless communication

Introduction

The rapid development of modern wireless communication technologies has led to shortage of spatial and spectral resources, bringing enormous challenges to the wireless communications. This issue has promoted the adoption of multiplexing, which is commonly used in computer networks and telecommunications. In the microwave, terahertz, and optical regions, signal multiplexing methods include space, angle, polarization, frequency, and orbital angular momentum multiplexing.[1–6] In the traditional wireless communications, these multiplexing methods require source coding, channel coding, and physical circuits, which make the hardware design and software complicated, and reduce the resource utilization. In addition, as the system becomes more complicated, the overhead for maintaining system synchronization and stability will increase. Therefore, novel wireless communication architectures are required to fully leverage the multiplexing.

Digital coding and programmable metasurfaces provide broad interfaces between digital information and physical worlds, showing promise for the next generation of smart wireless communications.[7–11] By customizing the electromagnetic (EM) properties of periodically or non-periodically arranged subwavelength meta-atoms using field-programmable gate array (FPGA), the wave propagation and wave-matter interaction can be dynamically manipulated for applications such as hologram imaging, anomalous reflection/refraction, and polarization

control.[7,12–16] More importantly, the digital coding characterization allows to map the EM wave parameters to digital information using the coding sequences to support metasurface-based information transmissions.[11,17–20] Further, time-domain digital coding metasurfaces have been proposed to enable nonlinear harmonic spectral reconfiguration,[21–32] bringing new degrees of freedom for the metasurface-based wireless communications. Currently, various wireless communication systems have been realized to directly modulate digital information onto the carrier waves by metasurfaces themselves and transmit the modulated signals to free space.[11,18,22,33–40] This information transmission strategy does not need the digital-to-analog convertor, radio-frequency (RF) mixer, and transmitting antenna, which greatly simplifies the frame of the traditional transmitters and reduces the hardware costs.

However, most of the existing metasurface-based communication systems have only one channel for information transmissions, and the amount of transmitted information is limited. To solve the above problem, a polarization modulation scheme was proposed using a polarization-controllable digital coding metasurface to realize dual-channel communications by shifting the incident frequencies of the metasurface at different time slots.[19] However, such a dual-channel communication scheme requires the changed incident frequencies with time, resulting in very low spectrum utilization of system and great difficulty in integrating the RF front-ends. Besides that, some prototypes of 2×2 multiple-input multiple-output (MIMO) wireless transmission systems based on the metasurfaces have been developed to transmit the information through two channels simultaneously.[41,42] But these works only achieved single-frequency signal transmissions, which neglected the potentials of STC digital metasurfaces for manipulating the signals and beams at the same time. In addition, the MIMO transmission requires joint demodulations of multiple received signals, and hereby increases the system complexity. Thereafter, an STC-metasurface wireless communication system based on space- and frequency-division multiplexing has been proposed to transmit multiple information streams to terminals at various locations simultaneously and independently via

different frequencies,[43] where the key is to optimize the STC matrices in real time to control the harmonic power intensities in different directions. Nevertheless, the design and optimization of the STC matrices will increase the design difficulty of the information modulation, which are hard to satisfy the requirements of real-time applications.

To improve the channel capacity and space utilization of the wireless communication systems and reduce the complexity, here we propose a space-frequency-polarization-division multiplexed wireless communication system using an anisotropic STC digital metasurface. We firstly present a polarization-division multiplexed (PDM) architecture to achieve independent signal modulations in two orthogonal directions using the anisotropic STC digital metasurface. To detect and separate different signals and increase the system capacity, we modulate the signals from two polarization channels onto different harmonic waves, achieving frequency-polarization-division multiplexed modulations. Subsequently, time-delay gradients are introduced in the control signals on the rows and columns of the metasurface for dynamic dual-harmonic beamforming along two polarization directions, realizing space-frequency-polarization-division multiplexed modulations. For experimental validations, we make two experiments. We firstly demonstrate the independent and synchronous video transmissions based on frequency-polarization-division multiplexed scheme. Then we further validate the performance of the space-frequency-polarization-division multiplexed scheme along the two polarization directions. The experimental results confirm the applicability of the proposed wireless communication system to multi-user scenarios.

Results

Polarization-division multiplexed architecture using anisotropic STC digital metasurface. We present a PDM architecture using the anisotropic STC digital metasurface, as illustrated in Fig. 1. Each metasurface element is composed of two parts that independently control the *x*- and *y*-polarized EM properties by sharing the aperture. A linearly polarized

plane wave radiated by a feed source, whose polarization direction is not parallel to both *x* and *y* axes (e.g., a 45° linearly polarized wave), serves as the incident wave to normally illuminate the metasurface. Owing to the anisotropic EM property, the metasurface can decompose the incident electric-field vector into two orthogonal components, thereby obtaining *x*- and *y*-polarized branches. Due to their inherent orthogonality, two independent reflected waves are generated simultaneously by the anisotropic STC digital metasurface. If the reflection coefficients in the two polarization directions (including their amplitudes and phases) can be adjusted in real time, we can realize independent controls to the amplitude and phase spectra for the *x*- and *y*-polarized reflected waves, along with independent signal modulations for a pair of orthogonally polarized EM waves. Hence, we can perform the PDM signal transmission using the anisotropic STC digital metasurface.

The dual-polarized reflection property of the anisotropic STC digital metasurface can be described by Jones matrix $\boldsymbol{H}(\boldsymbol{t})$, which is a 2 × 2 complex matrix expressing the relationship between the two orthogonal electric-field components in the time domain at the incidence and reflection:[29]

$$\boldsymbol{H}(\boldsymbol{t}) = \begin{bmatrix} \Gamma_{xx}(t) & \Gamma_{xy}(t) \\ \Gamma_{yx}(t) & \Gamma_{yy}(t) \end{bmatrix}, \tag{1}$$

where Γ_{xx} and Γ_{yy} are co-polarized reflection coefficients for the x and y polarizations, respectively. Assuming that the metasurface elements have extremely high cross-polarization isolation, the cross-polarized reflection coefficients can be simplified as $\Gamma_{xy} = \Gamma_{yx} = 0$. We express Γ_{xx} and Γ_{yy} in phasor notations, then $\boldsymbol{H}(\boldsymbol{t})$ is rewritten as

$$\boldsymbol{H}(\boldsymbol{t}) = \begin{bmatrix} |\Gamma_{xx}(t)|e^{j\Phi_{xx}(t)} & 0 \\ 0 & |\Gamma_{yy}(t)|e^{j\Phi_{yy}(t)} \end{bmatrix}, \tag{2}$$

where $|\Gamma(t)|$ and $\Phi(t)$ are the amplitude and phase of $\Gamma(t)$, respectively. Hence, the dual-polarized reflection process can be characterized by

$$\boldsymbol{E_r}(\boldsymbol{t}) = \boldsymbol{H}(\boldsymbol{t}) \cdot \boldsymbol{E_i}(\boldsymbol{t}). \tag{3}$$

Both notation vectors $\boldsymbol{E_i(t)}$ and $\boldsymbol{E_r(t)}$ consist of two elements, indicating the two polarization components: $\boldsymbol{E_i(t)} = \begin{bmatrix} E_{ix}(t) \\ E_{iy}(t) \end{bmatrix}$ and $\boldsymbol{E_r(t)} = \begin{bmatrix} E_{rx}(t) \\ E_{ry}(t) \end{bmatrix}$. Since Eq. (3) is similar to the reflection relation in the single-polarized mode,[17,18,22,35–38,41,43] the existing metasurface-based wireless communication systems can be easily adapted to the PDM operation.

Frequency-polarization-division multiplexed modulations based on the anisotropic STC digital metasurface. From Eq. (2), it is clear that the simultaneous and independent control of the time-varying co-polarized reflection coefficients Γ_{xx} and Γ_{yy} is the basis to realize the PDM wireless communications. According to the principle of the metasurface-based wireless communication,[17,35] we can simultaneously modulate the signals (both amplitude and phase) on each polarization channel by establishing the relation between the digital symbols and reflection coefficients of the metasurface. Moreover, considering the mapping relation in Refs. [22,36,41] and adopting a series of time-varying reflection coefficients as the symbols in different time slots, we can realize the PDM frequency modulation, PDM harmonic amplitude/phase modulations, and even more sophisticated high-order PDM signal modulations.

To separate multiple signals from different polarization channels, simplify independent multi-stream demodulations at the receiver end, and improve the system capacity, we propose a frequency-polarization-division multiplexed modulation scheme to carry two differently polarized signal streams through two carrier waves at different frequencies. In this way, the modulated waves can be easily distinguished and independently demodulated without requiring the joint demodulations in the MIMO wireless communication systems.

For example, we consider frequency-polarization-division multiplexed multiple phase-shift keying (MPSK) modulation for two polarized receivers through harmonic frequencies $f_c - f_0$ and $f_c + f_0$. For efficient harmonic signal modulation at a fixed polarization, a type of

time-varying reflection coefficient $\Gamma(t)$ with linearly varied phase over time is used, as shown in Fig. 2a. Its instantaneous expression in one period is expressed as

$$\Gamma(t) = Ae^{j(\varphi_1 + \frac{\Delta\varphi}{T} \cdot t)}, \ \ 0 \le t \le T, \tag{4}$$

where A is the magnitude of $\Gamma(t)$, T is the period of the symbol, and φ_1 and $\Delta\varphi$ are the initial phase state and phase difference, respectively. For the reflection-type metasurface with low return loss, A can be regarded as a constant at any time t. Under the normal radiation of the monochromatic plane wave $E_i(t) = e^{j\omega_c t}$ (where $\omega_c = 2\pi f_c$ is the angular frequency of the incident wave), the reflected wave $E_r(\omega)$ will be distributed at harmonic frequencies. The derivation of the specific harmonic amplitude/phase distribution is available in Supplementary Note 1. Fig. 2b gives the harmonic amplitude distributions with different phase differences $\Delta\varphi$, and Fig. 2c shows the energy conversion efficiencies of the $+1^{st}$, 0^{th}, and -1^{st} harmonics according to $\Delta\varphi$ with the reflection amplitude A = 1. We observe that more efficient signal modulations at the $+1^{st}$ harmonic can be achieved by increasing $\Delta\varphi$. On the contrary, if $\Delta\varphi$ is negative and $\Delta\varphi < -\pi$, as $\Delta\varphi$ decreases, the signal modulation is the most efficient at the -1^{st} harmonic. Therefore, the reflection function $\boldsymbol{H(t)}$ of the meta-atom for frequency-polarization-division multiplexed signal modulations in a period can be expressed as

$$\boldsymbol{H(t)} = \begin{bmatrix} A_x e^{j\Delta\varphi(1-\frac{t}{T})} & 0 \\ 0 & A_y e^{j\Delta\varphi\frac{t}{T}} \end{bmatrix}, \ \ 0 \le t \le T, \tag{5}$$

where A_x and A_y represent the co-polarized reflection amplitudes along the x and y directions, respectively. Hence, the x- and y-polarized signal modulations can be implemented at the frequencies $f_c - f_0$ and $f_c + f_0$, respectively.

To perform the MPSK modulations at the desired harmonics, the harmonic multi-bit phases must be precisely controlled. To this end, we introduce time delay t_d into the time-varying reflection coefficient, as shown by the solid line in Fig. 2a. The reflection coefficient with time delay t_d over one period can be expressed as

$$\Gamma(t-t_d)=\begin{cases}Ae^{j[\varphi_1+\frac{\Delta\varphi}{T}\cdot(t+T-t_d)]}, & 0\le t\le t_d\\ Ae^{j[\varphi_1+\frac{\Delta\varphi}{T}\cdot(t-t_d)]}, & t_d<t\le T\end{cases}. \tag{6}$$

Using the Fourier transform $\mathcal{F}[\Gamma(t-t_d)]=e^{-j\omega t_d}\Gamma(j\omega)$, we obtain the k^{th} harmonic phase increment as $\Delta\Phi|_{f_c+kf_0}=-k\omega_0 t_d$, while the harmonic energy remains unchanged.[26] Fig. 2d shows the phase delays of the $+1^{\text{st}}$, 0^{th}, and -1^{st} harmonics according to the time delay t_d. Therefore, a series of time-delayed reflection coefficients with proper t_d in two polarizations enable the frequency-polarization-division multiplexed MPSK modulation. The allocation strategy of the modulation signal sets for the two polarization channels is detailed in Supplementary Note 2. Then, the *x*-polarized MPSK modulation occurs at the -1^{st} harmonic, and the *y*-polarized MPSK modulation occurs simultaneously at the $+1^{\text{st}}$ harmonic, thus providing a general paradigm for rapid design of frequency-polarization-division multiplexed MPSK modulations.

Space-frequency-polarization-division multiplexed modulation with wide-angle coverage along two polarization directions. Eq. (5) describes the reflection function of the meta-atom for frequency-polarization-division multiplexed modulations. If all elements of the metasurface share the same reflection coefficient, the communication can be implemented in a finite region around the normal of the metasurface, leading to low space utilization rate. Hence we expect to implement space-frequency-polarization-division multiplexed modulations along two polarization directions by fully exploiting the harmonic beamforming of the anisotropic STC digital metasurface.

To perform the harmonic beamforming, we should design the phase profile at the target harmonic.[44,45] As shown in Fig. 2d, an arbitrary harmonic phase profile can be obtained by constructing the corresponding time-delay gradients on the reflection coefficients of all meta-atoms. Consider a general case as an example. We firstly divide the anisotropic STC digital metasurface into *M* rows and *N* columns to independently control the *x*-polarized EM property

of the same column, and the *y*-polarized EM property of the same row. Then we separately set independent time-delay gradient functions $tg1(x)$ and $tg2(y)$ in the *x* and *y* directions, among the control signals of different columns and rows, as shown in Fig. 1. Thus the reflection function $\boldsymbol{H}(\boldsymbol{t})$ of each meta-atom can be written as

$$\boldsymbol{H}(\boldsymbol{t},\boldsymbol{x},\boldsymbol{y}) = \begin{bmatrix} \Gamma_x[t - tg1(x)] & 0 \\ 0 & \Gamma_y[t - tg2(y)] \end{bmatrix}, \ 0 \le t \le T, \tag{7}$$

where $\Gamma_x[t - tg1(x)]$ and $\Gamma_y[t - tg2(y)]$ are given by Eq. (6). Referring to the classic antenna array theory, the harmonic phase profiles produced by the time-delay gradients $tg1(x)$ and $tg2(y)$ make the -1^{st} *x*-polarized and $+1^{st}$ *y*-polarized harmonic beams be deflected to the angle θ_x on the *xoz* plane and θ_y on the *yoz* plane, respectively: [30]

$$\theta_x = arcsin\left\{\frac{cf_0}{f_c - f_0}\frac{d[tg1(x)]}{dx}\right\}, \tag{8a}$$

$$\theta_y = arcsin\left\{-\frac{cf_0}{f_c + f_0}\frac{d[tg2(y)]}{dy}\right\}, \tag{8b}$$

where *c* is the light speed in vacuum, $f_0 = \frac{1}{T}$ is the frequency of the control signals, and $\frac{d(\cdot)}{dx}$ and $\frac{d(\cdot)}{dy}$ denote the derivatives with respect to positions *x* and *y*, respectively. Consequently, dynamic dual-harmonic beamforming along two polarization directions can be performed by independently switching $tg1(x)$ and $tg2(y)$.

As an intuitive example of dynamic dual-harmonic beamforming along two polarization directions, we consider an anisotropic STC digital metasurface composed of 12 × 12 meta-atoms ($M = N = 12$) with the following configuration parameters: f_c = 2.7 GHz, T = 2 μs, and the distances between two adjacent rows and columns with 36 *mm* (0.324 λ_c) and 25 *mm* (0.225 λ_c), respectively, where λ_c is the wavelength of the incident wave. In the *x* polarization direction, we enable five groups of time-delay gradients to $tg1(x)$, which are in turn:

$(\frac{3T}{4}, \frac{T}{2}, \frac{T}{4}, 0, \frac{3T}{4}, \frac{T}{2}, \frac{T}{4}, 0, \frac{3T}{4}, \frac{T}{2}, \frac{T}{4}, 0)$, $(\frac{2T}{3}, \frac{2T}{3}, \frac{T}{3}, \frac{T}{3}, 0, 0, \frac{2T}{3}, \frac{2T}{3}, \frac{T}{3}, \frac{T}{3}, 0, 0)$, $(0,0,0,0,0,0,0,0,0,0,0,0)$, $(0,0, \frac{T}{3}, \frac{T}{3}, \frac{2T}{3}, \frac{2T}{3}, 0, 0, \frac{T}{3}, \frac{T}{3}, \frac{2T}{3}, \frac{2T}{3})$, and $(0, \frac{T}{4}, \frac{T}{2}, \frac{3T}{4}, 0, \frac{T}{4}, \frac{T}{2}, \frac{3T}{4}, 0, \frac{T}{4}, \frac{T}{2}, \frac{3T}{4})$;

meanwhile, we apply the following group of time-delay gradients for *tg*2(*y*) along the *y* polarization direction, which are in turn:

$(0,0,\frac{T}{3},\frac{T}{3},\frac{2T}{3},\frac{2T}{3},0,0,\frac{T}{3},\frac{T}{3},\frac{2T}{3},\frac{2T}{3})$, $(0,0,0,\frac{T}{4},\frac{T}{4},\frac{T}{4},\frac{T}{2},\frac{T}{2},\frac{T}{2},\frac{3T}{4},\frac{3T}{4},\frac{3T}{4})$, (0,0,0,0,0,0,0,0,0,0,0,0),

$(\frac{3T}{4},\frac{3T}{4},\frac{3T}{4},\frac{T}{2},\frac{T}{2},\frac{T}{2},\frac{T}{4},\frac{T}{4},\frac{T}{4},0,0,0)$, and $(\frac{2T}{3},\frac{2T}{3},\frac{T}{3},\frac{T}{3},0,0,\frac{2T}{3},\frac{2T}{3},\frac{T}{3},\frac{T}{3},0,0)$,

as illustrated from the left to right in Fig. 3a (*x* polarization) and 3c (*y* polarization). According to Eq. (8a) and (8b), we can synthesize the -1^{st} *x*-polarized and $+1^{st}$ *y*-polarized beams in the directions of (θ_x, θ_y) on two polarization directions, as illustrated in Fig. 3b and 3d, which are in sequence of (−50.5°, −47.8°), (−31.0°, −21.7°), (0°, 0°), (+31.0°, +21.7°), and (+50.5°, +47.8°).

In the proposed modulation scheme, we use a single metasurface to achieve dynamic dual-harmonic beamforming along two polarization directions. Once the control signals of all columns and rows on the metasurface correspond to the MPSK symbols with the time-delay gradients *tg*1(*x*) and *tg*2(*y*) belonging to the modulation signal sets, as shown in Eq. (S3a)-(S3d) of Supplementary Note 2, space-frequency-polarization-division multiplexed MPSK modulations with wide-angle coverages are achieved on the two polarization directions.

Design of the anisotropic STC digital metasurface. Fig. 4a shows the element diagram of the proposed anisotropic STC digital metasurface.[29] The top metal pattern on the element mainly consists of two orthogonal shared-aperture rectangular patch pairs, which are printed on a grounded F4B substrate 1 ($\epsilon_r = 2.65$, $tan\ \delta = 0.0015$). Two varactor diodes (Skyworks SMV-1405) are embedded in the gap between the patch pairs, and two groups of metal strips are used to bias the varactors. To control the working states of the varactors independently, one group of metal strips is arranged on the top layer, while the other is arranged on the back of F4B substrate bonded with substrate 1. The patch pair is connected through two metal via holes. In addition, filtering inductors (27 nH) are introduced in the biasing strips to prevent high-frequency surface currents from entering the control circuit module. Detailed geometric

parameters of this programmable element are shown in Fig. 4b and Table 1.

Full-wave numerical simulations were conducted using the commercial software, CST Microwave Studio 2016. In element simulations, infinite periodic boundary conditions were adopted, and *x*- and *y*-polarized plane waves were used to normally illuminate the element along the −*z* direction to calculate the reflection properties. In the simulation, the varactors are modeled as lumped elements with R-L-C series circuit models, and the effective parameters are listed in Supplementary Table S1.

To demonstrate the EM properties of the anisotropic STC digital metasurface, Fig. 4c and 4d illustrate the simulated surface current distributions of the element at 2.7 GHz when radiated by the *x*- and *y*-polarized EM waves, respectively. We observe that a large amount of surface currents circulate through the diode that is parallel to the incident electric field. When the working state of the diode is altered, the phase of co-polarized reflected wave component changes. However, when the working state of the other diode is changed synchronously, owing to the minimal surface current nearby, the element cannot excite orthogonally polarized wave. This behavior suggests an excellent polarization isolation of the element, and hence the two diodes can independently control the phases of the *x*- and *y*-polarized reflected waves. To confirm the polarization isolation, we set *x*- and *y*-polarized waves to illuminate the element simultaneously and calculate the cross-polarized reflection coefficients at different voltages. For an arbitrary combination of the biasing voltages, the cross-polarized reflection amplitude remain below −50 dB, confirming the high polarization isolation of the element.

Fig. 4e shows the simulated reflection amplitudes and phases according to the biasing voltage of the anisotropic STC digital metasurface at 2.7 GHz, which verify the amplitude fluctuations and phase coverages of two co-polarized reflections. When the biasing voltage varies from 0 to 19 V, the phase ranges are approximately 200°, and the amplitudes varied within 1 dB for both *x*- and *y*-polarized reflected waves. Hence, the high polarization isolation and polarization-independent phase-shifting properties of the element comply with our design.

MPSK wireless communication system for frequency-polarization-division multiplexing. Firstly, we set up an MPSK wireless communication system based on frequency-polarization-division multiplexing with the proposed anisotropic STC digital metasurface in an indoor environment. We consider 16PSK signal modulation, in which the phase difference of the modulation signals $\Delta\varphi = 200^{\mathrm{o}}$, and the symbol period T = 2 μs. The modulation signals for the *x*- and *y*-polarization channels are given by Eq. (S5a) and (S5b) in Supplementary Note 2, respectively. According to Eq. (S2) in Supplementary Note 1, the *x*- and *y*-polarized harmonic energy ratios, $\frac{|\vec{E}_{rx}(\omega_c-\omega_0)|^2}{|\vec{E}_{rx}(\omega_c+\omega_0)|^2}$ and $\frac{|\vec{E}_{ry}(\omega_c+\omega_0)|^2}{|\vec{E}_{ry}(\omega_c-\omega_0)|^2}$, are both 10.9 dB, ensuring that the frequency channel of the -1^{st} harmonic is almost for the *x*-polarized wave, whereas the *y*-polarized wave is dominant in the frequency channel of the $+1^{st}$ harmonic.

Fig. 5a shows the indoor wireless communication scenario, and a schemetic diagram of the proposed communication system is presented in Supplementary Fig. S2. During the information transmission, two independent information sources are separately encoded into two sets of binary bit streams by the transmitter. The streams are then converted into two control signal sequences to drive the anisotropic STC digital metasurface through a customized control platform. Under the radiation of a 45°-tilted horn antenna with an incident frequency of 2.7 GHz, the metasurface will simultaneously reflected the -1^{st} *x*-polarized and $+1^{st}$ *y*-polarized modulated waves. At the receiver, a dual-polarized horn antenna with good polarization isolation receive the *x*- and *y*-polarized modulated signals at the distance of 3.5m, and transmit the signals to a commercial software-defined radio platform to recover the original information. More details on the information transmission and system equipment are avaliable in Supplementary Note 4. In the baseband signal processing, the conventional communication methods such as least square channel estimation and zero forcing channel equalization are used at the receiver to compensate for the channel fading.

Fig. 5b shows the independent and synchronous transmissions of two 480p resolution

(640 × 480) videos through the proposed frequency-polarization-division multiplexed MPSK communication system. During the video transmission, the two 16PSK constellations for the 2.6995 GHz *x*-polarized and 2.7005 GHz *y*-polarized channels remain stable, and the transmissions of Videos 1 and 2 have very good quality (see Supplementary Video 1 for details). Furthermore, as shown in Fig. 5c, when one channel (e.g., the 2.6995 GHz *x*-polarized channel) is disabled, the corresponding constellation disappears and the video recovery is interrupted, but the remaining video transmission continues without interference, showing the independent transmissions of the two videos (see Supplementary Video 1 for details). Thus, the proposed communication system operates very well as expected with a transmission rate up to 20 Mbps.

MPSK wireless communication system for the space-frequency-polarization-division multiplexing. Before experimentally demonstrating the space-frequency-polarization-division multiplexed MPSK communication system, we firstly show that the anisotropic STC digital metasurface coulf perform dynamic dual-harmonic beamforming along the two polarization directions. The experimental setup is detailed in Supplementary Note 5. We assign the time-varying reflection coefficients $\Gamma_{xx}(t) = \Gamma_x[t - tg1(x)]$ and $\Gamma_{yy}(t) = \Gamma_y[t - tg2(y)]$ to the columns and rows of the metasurface, in which $tg1(x)$ and $tg2(y)$ are illustrated in Fig. 3a and 3c, respectively.

Fig. 6a and 6b show the normalized far-field scattering patterns of the -1^{st} *x*-polarized and $+1^{st}$ *y*-polarized waves under the five groups of time-delay gradients $tg1(x)$ and $tg2(y)$, which indicate that the beam directions are consistent with theoretical predictions. We observe that the harmonic beam directions of two polarizations and two frequencies can be freely manipulated, supporting the capability of space-frequency-polarization-division multiplexing.

We conduct a simple indoor experiment to verify the effectiveness of the proposed

space-, polarization-, and frequency-division multiplexed MPSK communication system. We use quadrature phase-shift keying (QPSK) modulation in the system, where the modulation signal sets for the x and y polarization channels are given by Eq. (S4a) and (S4b) in Supplementary Note 2, respectively. The other parameters are the same as those described in the simulations. The experimental setup is shown in Fig. 6c. For the transmitter, we assign the time-delay gradients $tg1(x)$ and $tg2(y)$ as:

$$(0,\frac{T}{4},\frac{T}{2},\frac{3T}{4},0,\frac{T}{4},\frac{T}{2},\frac{3T}{4},0,\frac{T}{4},\frac{T}{2},\frac{3T}{4}) \text{ and } (\frac{3T}{4},\frac{3T}{4},\frac{3T}{4},\frac{T}{2},\frac{T}{2},\frac{T}{2},\frac{T}{4},\frac{T}{4},\frac{T}{4},0,0,0),$$

which are embedded into the control signal sequences of the columns and rows of the metasurface, respectively. The rest of the transmitter architecture is consistent with that described in the simulations. For the receivers, four horn antennas are fixed with different angles on the *xoz* and *yoz* planes to resemble four users with different receiving directions, as shown in Fig. 6c. Here, Users 1 and 2 are represented by the *x*-polarized antennas distributed on the *xoz* plane for angles of 50° and 25° with respect to the incident path; while Users 3 and 4 are represented by the *y*-polarized antennas distributed on the *yoz* plane for angles of −20° and 10° with respect to the incident path, respectively. The four antennas are equidistant from the metasurface at 3.5 m.

Fig. 6a and 6b demonstrate that the main beam lobe of the -1^{st} harmonic *x*-polarized scattering pattern is approximately at 50°, and that of the $+1^{st}$ harmonic *y*-polarized scattering pattern is approximately at −20°. From Fig. 6d and 6f, Users 1 and 3 can demodulate nearly perfect QPSK constellation points at 2.6995 GHz for the *x*-polarized channel and at 2.7005 GHz for the *y*-polarized channel, respectively, showing very excellent communication performance, since the users are located at the main beams directions of the two harmonics and polarizations. For Users 2 and 4, the corresponding constellation points become deteriorate, as illustrated in Fig. 6e and 6g, owing to the fact that the users are apart from the main beams and hence receive lower energies. Although the deteriorate constellation points

may result in higher bit error rate (BER), the two users (2 and 4) still receive relatively good communication quality because the constellation diagrams have good shapes for QPSK. The information transmission can be seen in Supplementary Video 2, and the BERs for Users 1-4 are shown in Supplementary Fig. S4. This experiment indicates that the performance of the space-frequency-polarization-division multiplexed MPSK communication system can be guaranteed.

Conclusion and discussion

We proposed an architecture for space-frequency-polarization-division multiplexed MPSK communications based on the anisotropic STC digital metasurface, which have been verified by two experiments. In the first experiment, wireless transmissions of two complete videos were demonstrated simultaneously in real time using the frequency-polarization-division multiplexed 16PSK scheme; while in the second experiment, the good performance of space-frequency-polarization-division multiplexed QPSK scheme was validated with dynamic dual-harmonic beamforming along the two polarization directions. We remark that the overall performance of the proposed system can be further enhanced by increasing the phase-varying range of meta-atom in two polarization directions, enlarging the number of controllable meta-atoms in the metasurface, and broadening the signal bandwidth of the amplifier circuits. In comparison with the conventional wireless communication systems, our proposal provides low costs and high integrations for the general metasurface-based wireless communication systems, and more importantly it improves the space utilization and channel capacities by using the space-frequency-polarization-division multiplexing. Hence the proposed theory, technology and system can be used in the low-cost and simple-architecture wireless communications for multiple users.

Data availability

The data that support the plots within this paper and other findings of this study are available from the corresponding author upon reasonable request.

References

[1] Gesbert, D., Shafi, M., Shiu, D. S., Smith, P. J. & Naguib, A. From theory to practice: An overview of MIMO space-time coded wireless systems. *IEEE J. Sel. Area Comm.* **21**, 281-302 (2003).

[2] Kamali, S. M., Arbabi, E., Arbabi, A., Horie, Y., Faraji-Dana, M. & Faraon, A. Angle-multiplexed metasurfaces: Encoding independent wavefronts in a single metasurface under different illumination angles. *Phys. Rev. X* **7**, 041056 (2017).

[3] Nabar, R. U., Bölcskei, H., Erceg, V., Gesbert, D. & Paulraj, A. J. Performance of multiantenna signaling techniques in the presence of polarization diversity. *IEEE Trans. Signal Process.* **50**, 2553-2562 (2002).

[4] Wang, Q. et al. Polarization and frequency multiplexed terahertz meta-holography. *Adv. Opt. Mater.* **5**, 1700277 (2017).

[5] Chen, S., Liu, W., Li, Z., Cheng, H. & Tian, J. Metasurface-empowered optical multiplexing and multifunction *Adv. Mater.* **32**, 1805912 (2020).

[6] Yan, Y. et al. High-capacity millimetre-wave communications with orbital angular momentum multiplexing. *Nat. Commun.* **5**, 4876 (2014).

[7] Cui, T. J., Qi, M. Q., Wan, X., Zhao, J. & Cheng, Q. Coding metamaterials, digital metamaterials and programmable metamaterials. *Light: Sci. Appl.* **3**, e218 (2014).

[8] Li, X. et al. Code division multiplexing inspired dynamic metasurface holography. *Adv. Funct. Mater.* **31**, 2103326 (2021).

[9] Han, Y., Tang, W., Jin, S., Wen, C. K. Ma, X. Large intelligent surface-assisted wireless communication exploiting statistical CSI. *IEEE Trans. Veh. Technol.* **68**, 8238-8242 (2019).

[10] Tao, J. et al. Mass-manufactured beam-steering metasurfaces for high-speed full-duplex optical wireless-broadcasting communications. *Adv. Mater.* **34**, 2106080 (2022).

[11] Cui, T. J., Liu, S., Bai, G. D. & Ma, Q. Direct transmission of digital message via programmable coding metasurface. *Research* **2019**, 1-12 (2019).

[12] Zhang, N. et al. Programmable Coding Metasurface for Dual-Band Independent Real-Time Beam Control. *IEEE J. Emerg. Sel. Topics Circuits Syst.* **10**, 20-28 (2020).

[13] Cong, L. et al. Active multifunctional microelectromechanical system metadevices: Applications in polarization control, wavefront deflection, and holograms. *Adv. Opt. Mater.* **5**, 1600716 (2017).

[14] Chen, K., Zhang, N., Ding, G., Zhao, J., Jiang, T. & Feng, Y. Active anisotropic coding metasurface with independent real-time reconfigurability for dual polarized waves. *Adv. Mater. Technol.* **5**, 1900930 (2020).

[15] Yang, H. et al. A programmable metasurface with dynamic polarization, scattering and focusing control. *Sci. Rep.* **6**, 35692 (2016).

[16] Liao, J., Guo, S., Yuan, L., Ji, C., Huang, C. & Luo, X. Independent manipulation of reflection amplitude and phase by a single-layer reconfigurable metasurface. *Adv. Opt. Mater.* **10**, 2101551 (2022).

[17] Ke, J. C., Jiang, Y. X., Chen, M. Z., Zhang, J. W. & Cheng, Q. An OOK wireless communication system based on transmissive digital coding metasurface. In *Proc. 2021 Cross Strait Radio Science and Wireless Technology Conference (CSRSWTC)*, 86-88 (2021**)**.

[18] Henthorn, S., Ford, K. L. & O'Farrell, T. Bit-error-rate performance of quadrature modulation transmission using reconfigurable frequency selective surfaces. *IEEE Antennas Wirel. Propag. Lett.* **16**, 2038-2041 (2017).

[19] Huang, C. X., Zhang, J., Cheng, Q. & Cui, T. J. Polarization modulation for wireless communications based on metasurfaces. *Adv. Funct. Mater.* **31**, 2103379 (2021).

[20] Wu, Q. & Zhang, R. Towards smart and reconfigurable environment: intelligent reflecting surface aided wireless network. *IEEE Commun. Mag.* **58**, 106-112 (2020).

[21] Yang, J. et al. Simultaneous conversion of polarization and frequency via time-division-multiplexing metasurfaces. *Adv. Opt. Mater.* **9**, 2101043 (2021).

[22] Zhao, J. et al. Programmable time-domain digital-coding metasurface for non-linear harmonic manipulation and new wireless communication systems. *Natl. Sci. Rev.* **6**, 231-238 (2019).

[23] Zhang, L. et al. Space-time-coding digital metasurfaces. *Nat. Commun.* **9**, 4334 (2018).

[24] Tennant, A. & Chambers, B. Time-switched array analysis of phase-switched screens. *IEEE Trans. Antennas Propag.* **57**, 808-812 (2009).

[25] Zhang, L. et al. Breaking reciprocity with space-time-coding digital metasurfaces. *Adv. Mater.* **31**, 1904069 (2019).

[26] Dai, J. Y. et al. High-efficiency synthesizer for spatial waves based on space-time-coding digital metasurface. *Laser Photon. Rev.* **14**, 1900133 (2020).

[27] Hadad, Y., Sounas, D. L. & Alu, A. Space-time gradient metasurfaces. *Phys. Rev. B* **92**, 100304 (2015).

[28] Taravati, S. & Eleftheriades, G. V. Full-duplex nonreciprocal beam steering by time-modulated phase-gradient metasurfaces. *Phys. Rev. Appl.* **14**, 014027 (2020).

[29] Ke J. C. et al. Linear and nonlinear polarization syntheses and their programmable controls based on anisotropic time-domain digital coding metasurface. *Small Struct.* **2**, 2000060 (2021).

[30] Zhang, C. et al. Convolution operations on time-domain digital coding metasurface for beam manipulations of harmonics *Nanophotonics* **9**, 2771-2781 (2020).

[31] Shaltout, A., Kildishev, A. & Shalaev, V. Time-varying metasurfaces and Lorentz non-reciprocity. *Opt. Mater. Express* **5**, 2459 (2015).

[32] Castaldi, G. et al. Joint multi-frequency beam shaping and steering via space–time-coding digital metasurfaces *Adv. Funct. Mater.* **31**, 2007620 (2021).

[33] Renzo, M. D. et al. Smart radio environments empowered by reconfigurable intelligent surfaces: How it works, state of research, and the road ahead. *IEEE J. Sel. Area Comm.* **38**, 2450-2525 (2020).

[34] Liaskos, C., Nie, S., Tsioliaridou, A., Pitsillides, A., Ioannidis, S. & Akyildiz, I. A new wireless communication paradigm through software-controlled metasurfaces. *IEEE Commun. Mag.* **56**, 162-169 (2018**)**.

[35] Dai, J. Y. et al. Wireless communications through a simplified architecture based on time-domain digital coding metasurface. *Adv. Mater. Technol.* **4**, 1900044 (2019).

[36] Chen, M. Z. et al. Accurate and broadband manipulations of harmonic amplitudes and phases to reach 256 QAM millimeter-wave wireless communications by time-domain digital coding metasurface. *Natl. Sci. Rev.* **9**, nwab134 (2022).

[37] Dai, J. Y. et al. Wireless communication based on information metasurfaces. *IEEE Trans. Microwave Theory Tech.* **69**, 1493-1510 (2021).

[38] Henthorn, S., Ford K. L. & O'Farrell, T. Direct antenna modulation for high-order phase shift keying. *IEEE Trans. Antennas Propag.* **68**, 111-120 (2020).

[39] Nie, S. & Akyildiz, I. F. Metasurfaces for multiplexed communication. *Nat. Electron.* **4**, 177-178 (2021).

[40] Yu, S., Liu, H. & Li, L. Design of near-field focused metasurface for high-efficient wireless power transfer with multifocus characteristics. *IEEE Trans. Ind. Electron.* **66**, 3993-4002 (2019).

[41] Tang, W. et al. MIMO transmission through reconfigurable intelligent surface: System design, analysis, and implementation. *IEEE J. Sel. Area Comm.* **38**, 2683-2699 (2020).

[42] Chen, X. et al. Design and implementation of MIMO transmission based on dual-polarized reconfigurable intelligent surface. *IEEE Wirel. Commun. Lett.* **10**, 2155-2159 (2021).

[43] Zhang, L. et al. A wireless communication scheme based on space- and frequency-division multiplexing using digital metasurfaces. *Nat. Electron.* **4**, 218-227 (2021).

[44] Yu, N. et al. Light propagation with phase discontinuities: Generalized laws of reflection and refraction. *Science* **334**, 333-337 (2011).

[45] Sun, S., He, Q., Xiao, S., Xu, Q., Li, X. & Zhou, L. Gradient-index meta-surfaces as a bridge linking propagating waves and surface waves. *Nat. Mater.* **11**, 426-431 (2012).

Acknowledgements

J. C. K. and X. C. contributed equally to this work. This work was supported by the National Key Research and Development Program of China (2017YFA0700201, 2017YFA0700202, and 2017YFA0700203), the National Natural Science Foundation of China (61631007, 61571117, 61138001, 61371035, 61722106, 61731010, 62101123, and 11227904), the 111 Project (111-2-05), the China Postdoctoral Science Foundation (2020M680062), the National Postdoctoral Program for Innovative Talents (BX2021062), and the National Science Foundation of China for Distinguished Young Scholars (61625106).

Author contributions

Q.C., S.J., and T.J.C. put forward the idea and provided the instructions for this work. J.C.K.,

X.C., Q.C., S.J., and T.J.C. conceived the designs and conducted the theoretical analyses and simulations. J.Y.D., M.Z.C., L.Z., and L.W. conducted parts of the designs and simulations. J.C.K., X.C., W.T., J.Y.D., and M.Z.C. devised the measurement system, performed the experiments, and interpreted the results, with J.Y., J.W.Z., and L.W. assisting. J.C.K., Q.C., S.J., and T.J.C. co-wrote the manuscript. All authors contributed to the writing and revising of the manuscript together.

Conflict of Interest

The authors declare no conflict of interest.

Additional information

Supplementary Information is available from the Online Library or from the authors.

Figure Captions

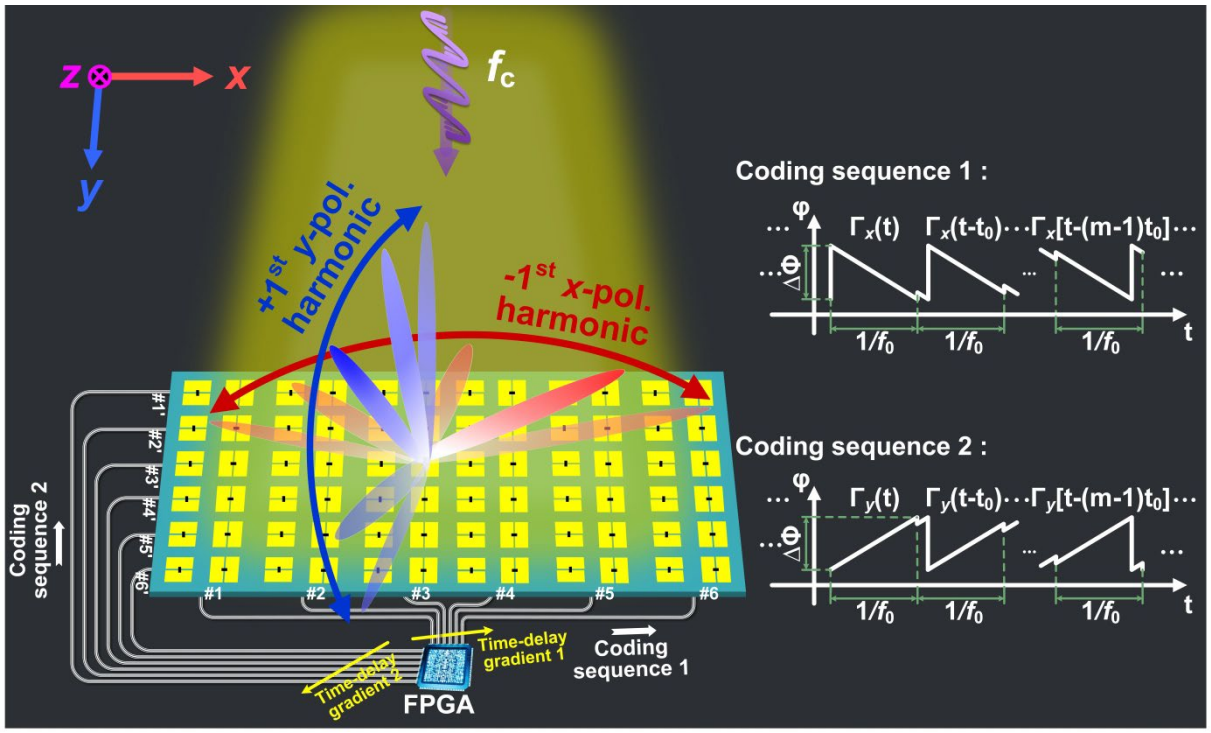

Fig. 1 | The space-frequency-polarization-division multiplexing architecture using anisotropic STC digital metasurface for simultaneously scanning harmonic beams at different frequencies on two orthogonal polarizations, which results in a low-cost and high-capacity wireless communication system. Coding sequences 1 and 2 are the basic time-varying control waveforms, which are used to drive the varactor diodes parallel to the *x* and *y* polarization directions. Different time-delay gradients 1 and 2 are added in the two coding sequences in different control lines with the same polarization.

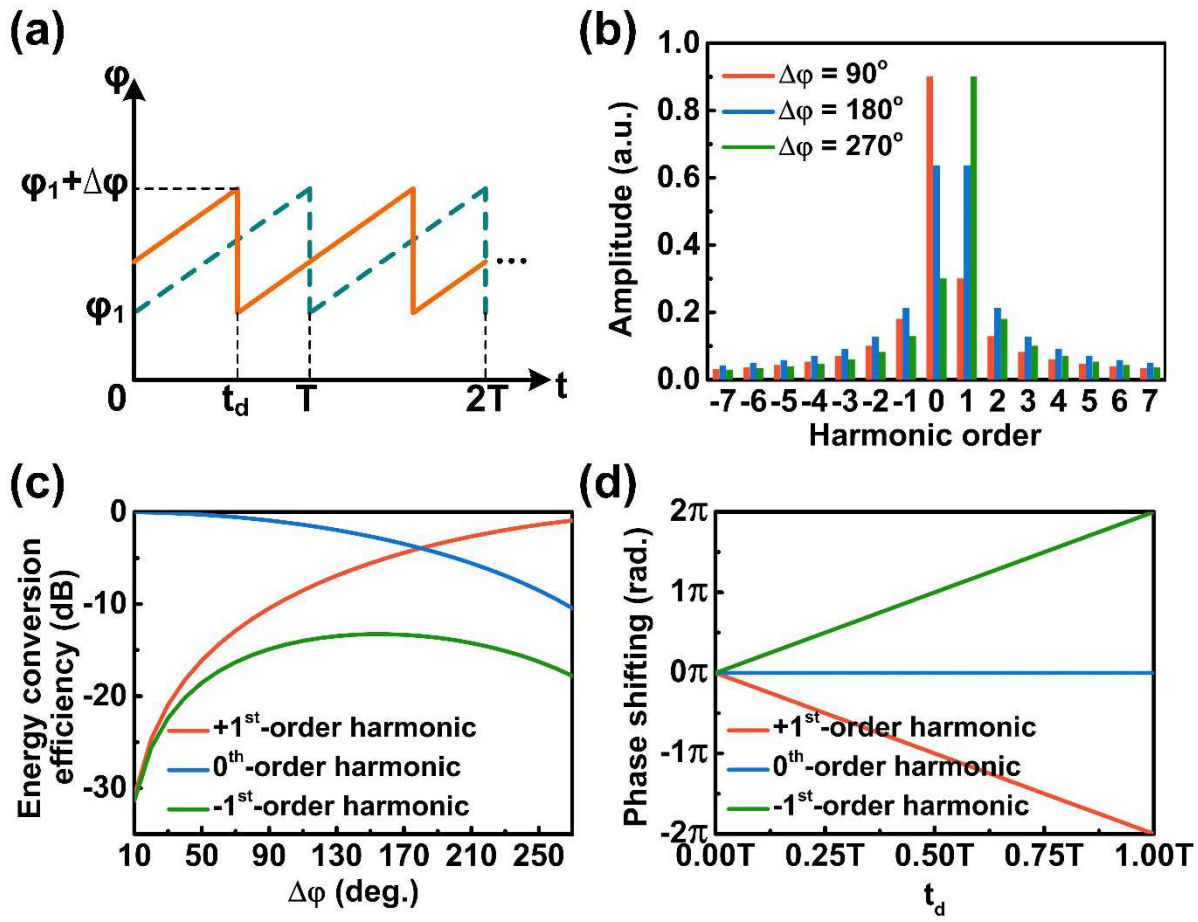

Fig. 2 | a, Time-varying phases of the original (dashed line) and time-delayed (solid line) reflection coefficients. **b,** Calculated harmonic amplitude distributions with phase differences ($\Delta\varphi$) of 90°, 180°, and 270°, respectively. **c,** Calculated energy conversion efficiencies of the $+1^{st}$, 0^{th}, and -1^{st} harmonics as the functions of $\Delta\varphi$. **d,** Calculated phase shifting of the $+1^{st}$, 0^{th}, and -1^{st} harmonics as the functions of time delay t_d.

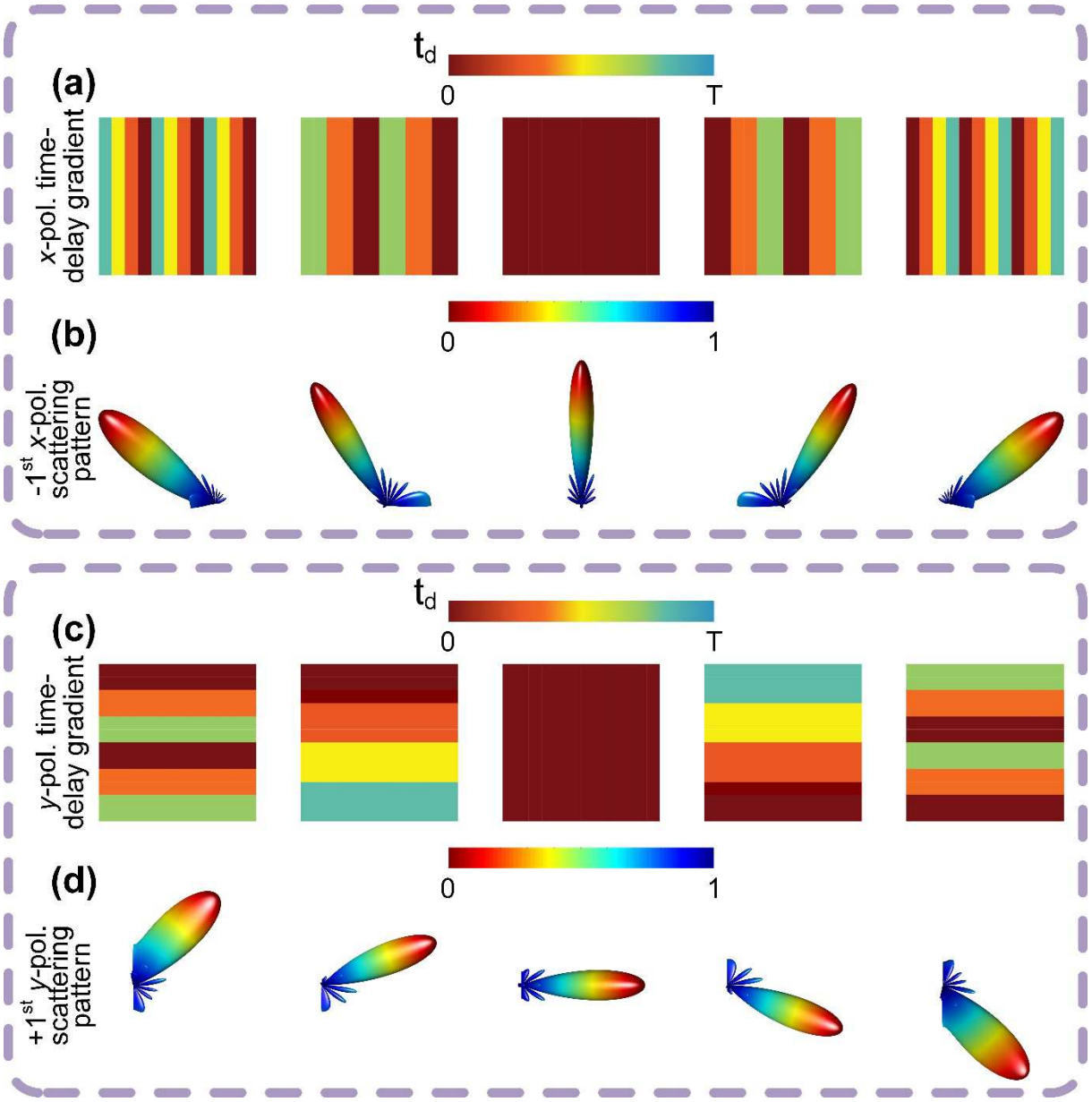

Fig. 3 | Dynamic harmonic beamforming along different polarization directions. a, Time-delay gradients $tg1(x)$ along the x polarization direction: $(\frac{3T}{4},\frac{T}{2},\frac{T}{4},0,\frac{3T}{4},\frac{T}{2},\frac{T}{4},0,\frac{3T}{4},\frac{T}{2},\frac{T}{4},0)$, $(\frac{2T}{3},\frac{2T}{3},\frac{T}{3},\frac{T}{3},0,0,\frac{2T}{3},\frac{2T}{3},\frac{T}{3},\frac{T}{3},0,0)$, $(0,0,0,0,0,0,0,0,0,0,0,0)$, $(0,0,\frac{T}{3},\frac{T}{3},\frac{2T}{3},\frac{2T}{3},0,0,\frac{T}{3},\frac{T}{3},\frac{2T}{3},\frac{2T}{3})$, and $(0,\frac{T}{4},\frac{T}{2},\frac{3T}{4},0,\frac{T}{4},\frac{T}{2},\frac{3T}{4},0,\frac{T}{4},\frac{T}{2},\frac{3T}{4})$. **b,** Scattering patterns of the -1^{st} x-polarized harmonic with beam directions of −50.5°, −31.0°, 0°, +31.0°, and +50.5° on the xoz plane. **c,** Time-delay gradients $tg2(y)$ along the y polarization direction: $(0,0,\frac{T}{3},\frac{T}{3},\frac{2T}{3},\frac{2T}{3},0,0,\frac{T}{3},\frac{T}{3},\frac{2T}{3},\frac{2T}{3})$, $(0,0,0,\frac{T}{4},\frac{T}{4},\frac{T}{4},\frac{T}{2},\frac{T}{2},\frac{T}{2},\frac{3T}{4},\frac{3T}{4},\frac{3T}{4})$, $(0,0,0,0,0,0,0,0,0,0,0,0)$, $(\frac{3T}{4},\frac{3T}{4},\frac{3T}{4},\frac{T}{2},\frac{T}{2},\frac{T}{2},\frac{T}{4},\frac{T}{4},\frac{T}{4},0,0,0)$, and $(\frac{2T}{3},\frac{2T}{3},\frac{T}{3},\frac{T}{3},0,0,\frac{2T}{3},\frac{2T}{3},\frac{T}{3},\frac{T}{3},0,0)$. **d,** Scattering patterns of the $+1^{st}$ y-polarized harmonic with beam directions of −47.8°, −21.7°, 0°, +21.7°, and +47.8° on the yoz plane.

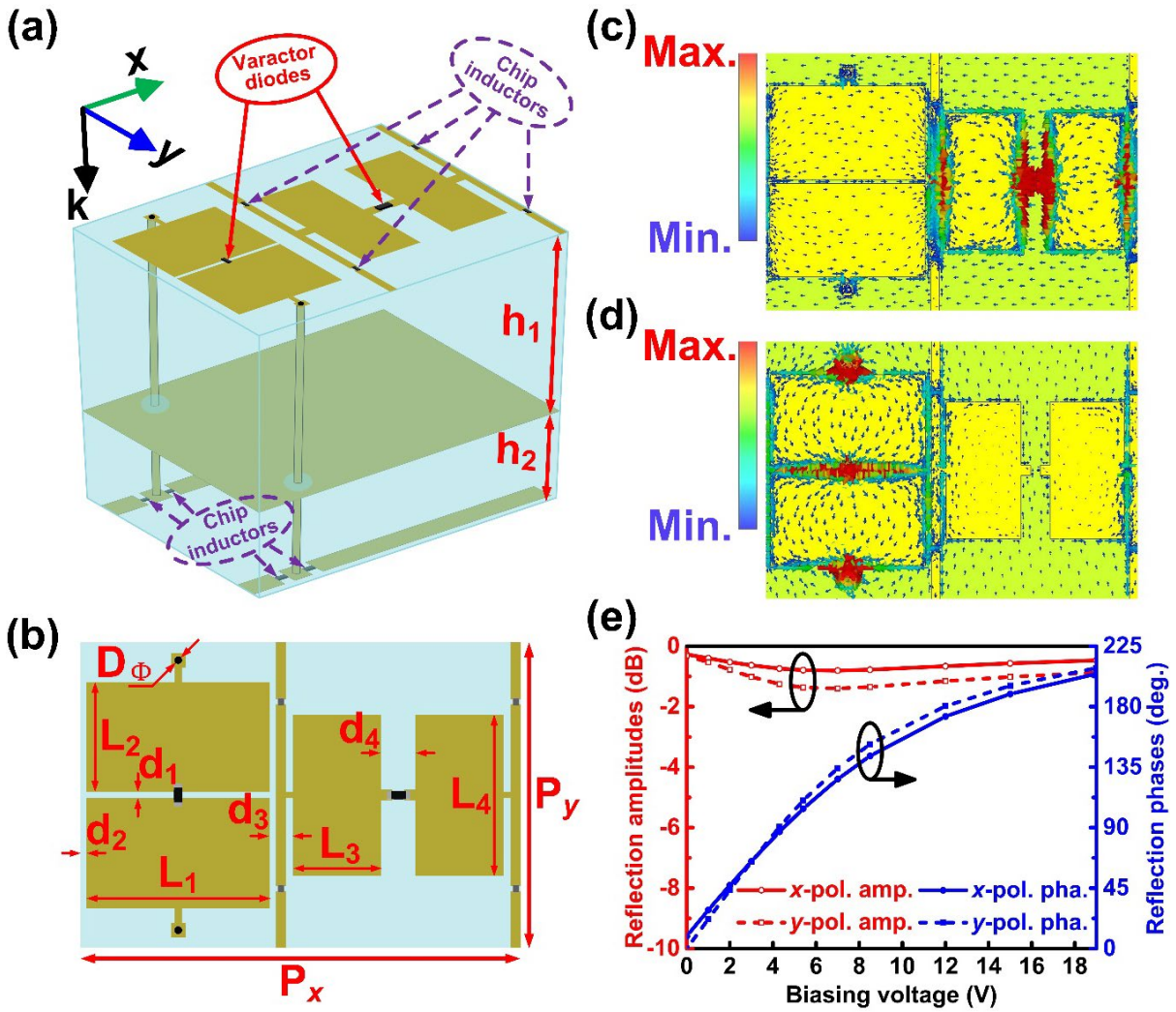

Fig. 4 | a, Unit element of the anisotropic STC digital metasurface. **b,** Top layer of the element and its geometrical parameters. **c-d,** Surface current distributions of the element when the metasurface is radiated by **(c)** *x*- and **(d)** *y*-polarized plane waves. **e,** Relation between the *x*- and *y*-polarized reflection properties of the metasurface and the biasing voltage at 2.7 GHz.

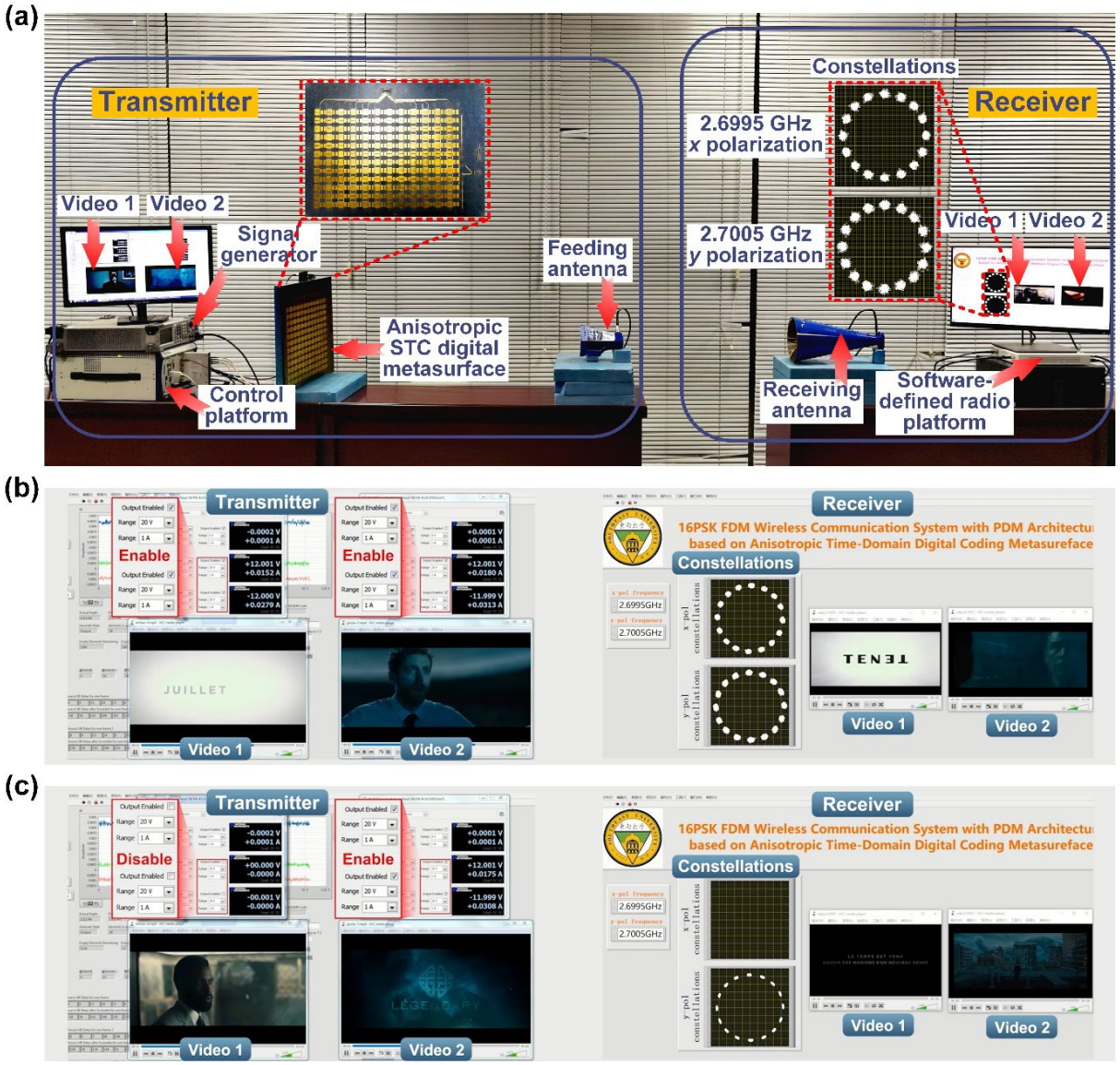

Fig. 5 | a, Experimental setup of the frequency-polarization-division multiplexed MPSK communication system. In the experiments, two 480p resolution (640 × 480) videos, which were separately modulated on 2.6995 GHz *x*-polarized and 2.7005 GHz *y*-polarized waves, are independently and synchronously transmitted from the transmitter (left) to the receiver (right). **b-c,** Experimental video transmission scenarios of the system when **(b)** dual channels are, and **(c)** only the 2.7005 GHz *y*-polarized channel is enabled, in which the 16PSK constellations of the dual channels **(b)** and only the 2.7005 GHz *y*-polarized channel **(c)** are very stable. In the dual-channel situation, the transmissions of videos 1 and 2 are very fluent; and in the later situation, only video 2 are fluently transmitted.

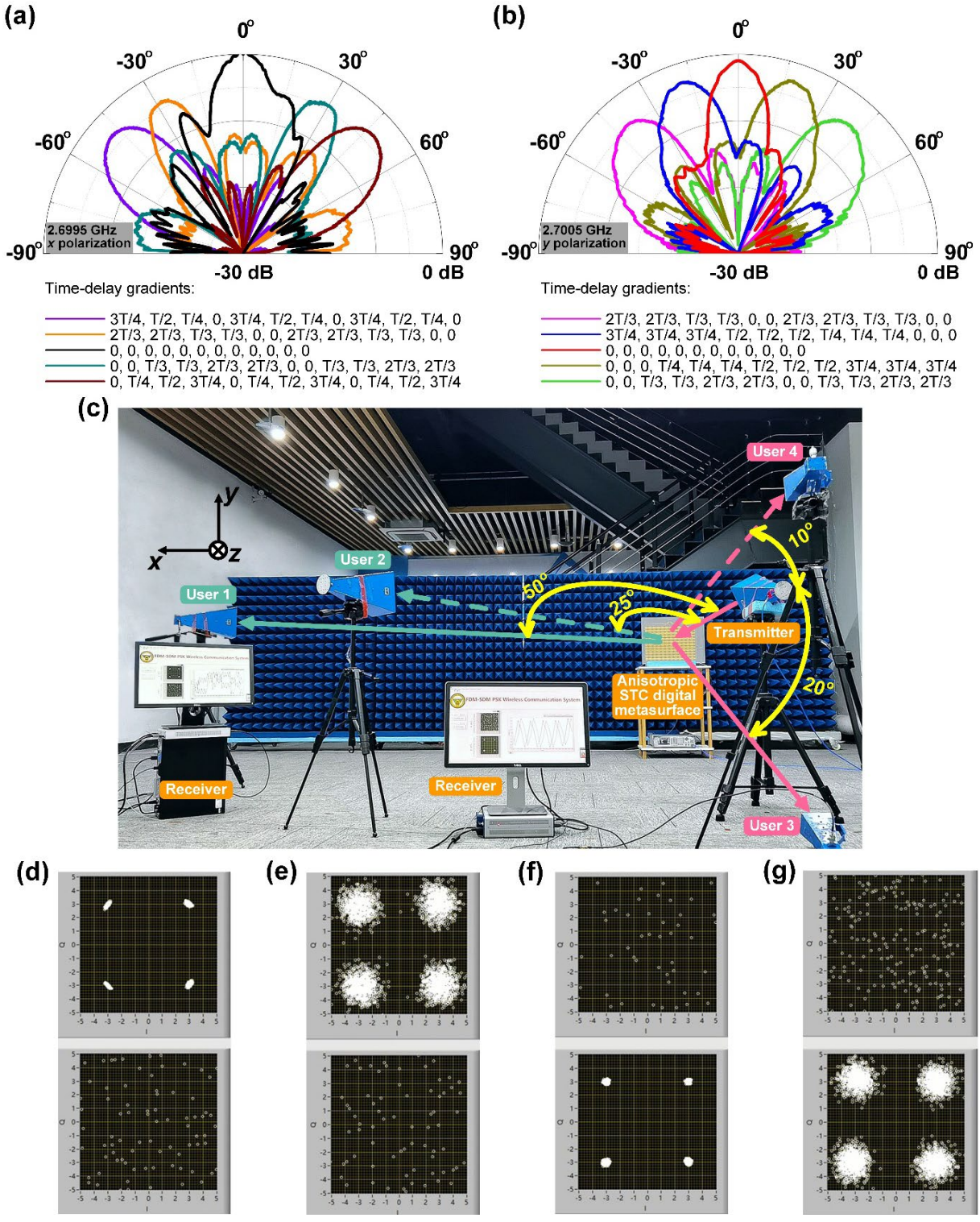

Fig. 6 | a-b, Normalized measured scattering patterns of 2.6995 GHz *x*-polarized **(a)** and 2.7005GHz *y*-polarized **(b)** harmonics. The five groups of (color-coded) time-delay gradients are chosen as the candidates for the dual-harmonic beamforming along the **(a)** *xoz* and **(b)** *yoz* polarization directions. **c,** Experimental setup of the space-frequency-polarization-division multiplexed MPSK communication system, in which Users 1 and 2 are located on the *xoz* plane, while Users 3 and 4 are located on the *yoz* plane. The four users point to different directions. **d-g,** QPSK constellations for Users 1-4. We note that two perfect QPSK

constellations are successfully demodulated for User 1 at the 2.6995 GHz *x*-polarized channel **(d)** and for User 3 at the 2.7005 GHz *y*-polarized channel **(f)**; while two imperfect constellations are demodulated for User 2 at the 2.6995 GHz *x*-polarized channel **(e)** and for User 4 at the 2.7005 GHz *y*-polarized channel **(g)**.

Table 1 | Dimensions of element in anisotropic STC digital metasurface.

Parameter	P_x	P_y	L_1	L_2	L_3	L_4	d_1	d_2	d_3	d_4	D_Φ	h_1	h_2
Value (mm)	36	25	15	9	7.2	13.2	0.4	0.5	2	2.8	0.6	5	2

Supplementary Files

This is a list of supplementary files associated with this preprint. Click to download.

- SupplementaryInformation.docx
- SupplementaryVideo1.mp4
- SupplementaryVideo2.mp4